

See discussions, stats, and author profiles for this publication at: <https://www.researchgate.net/publication/330366849>

Using field data-based large eddy simulation to understand role of atmospheric stability on energy production of wind turbines

Article in *Wind Engineering* · January 2019

DOI: 10.1177/0309524X18824540

CITATIONS

0

READS

133

2 authors:



Jordan Nielson

University of Texas at San Antonio

5 PUBLICATIONS 1 CITATION

[SEE PROFILE](#)



Kiran Bhaganagar

University of Texas at San Antonio

57 PUBLICATIONS 423 CITATIONS

[SEE PROFILE](#)

Some of the authors of this publication are also working on these related projects:




Detection and Tracking Gas plume using a heterogeneous network of unmanned systems [View project](#)



Density Currents Over Complex Bathymetry [View project](#)

Using field data–based large eddy simulation to understand role of atmospheric stability on energy production of wind turbines

Wind Engineering
2019, Vol. 43(6) 625–638
© The Author(s) 2019
Article reuse guidelines:
sagepub.com/journals-permissions
DOI: 10.1177/0309524X18824540
journals.sagepub.com/home/wie


Jordan Nielson  and Kiran Bhaganagar

Abstract

A novel and a robust high-fidelity numerical methodology has been developed to realistically estimate the net energy production of full-scale horizontal axis wind turbines in a convective atmospheric boundary layer, for both isolated and multiple wind turbine arrays by accounting for the wake effects between them. Large eddy simulation has been used to understand the role of atmospheric stability in net energy production (annual energy production) of full-scale horizontal axis wind turbines placed in the convective atmospheric boundary layer. The simulations are performed during the convective conditions corresponding to the National Renewable Energy Laboratory field campaign of July 2015. A mathematical framework was developed to incorporate the field-based measurements as boundary conditions for the large eddy simulation by averaging the surface flux over multiple diurnal cycles. The objective of the study is to quantify the role of surface flux in the calculation of energy production for an isolated, two and three wind turbine configuration. The study compares the mean value, +1 standard deviation, and –1 standard deviation from the measured surface flux to demonstrate the role of surface heat flux. The uniqueness of the study is that power deficits from large eddy simulation were used to determine wake losses and obtain a net energy production that accounts for the wake losses. The frequency of stability events, from field measurements, is input into the calculation of an ensemble energy production prediction with wake losses for different wind turbine arrays. The increased surface heat flux increases the atmospheric turbulence into the wind turbines. Higher turbulence results in faster wake recovery by a factor of two. The faster wake recovery rates result in lowering the power deficits from 46% to 28% for the two-turbine array. The difference in net energy production between the +1 and –1 standard deviation (with respect to surface heat flux) simulations was 10% for the two-turbine array and 8% for the three-turbine array. An ensemble net energy production by accounting for the wake losses indicated the overestimation of annual energy production from current practices could be corrected by accounting for variation of surface flux from the mean value.

Keywords

Energy production, wind turbine, surface heat flux, atmospheric boundary layer, large eddy simulation, probability density function, wind energy

Introduction

Annual energy production (AEP) is a key metric used when performing financial estimates for wind turbines and wind farms (Fingersh et al., 2006). AEP is an estimate of the annual energy produced by a wind turbine or a wind farm. Accurate prediction of energy production aids in reducing the overall cost of energy. AEP is further subdivided into AEP_{gross} and AEP_{net} (Xydis et al., 2009). AEP_{gross} is the estimated energy production without any losses. AEP_{net} is the estimated energy production including inefficiencies such as wake losses, mechanical/electrical losses, and blade losses. The most simplistic method for estimating AEP_{gross} is to use a wind turbine power curve (Sohoni et al., 2016). The power curve

Laboratory of Turbulence, Sensing and Intelligence Systems, Department of Mechanical Engineering, The University of Texas at San Antonio, San Antonio, TX, USA

Corresponding author:

Kiran Bhaganagar, Laboratory of Turbulence, Sensing and Intelligence Systems, Department of Mechanical Engineering, The University of Texas at San Antonio, One UTSA Circle, San Antonio, TX 78249, USA.
Email: Kiran.bhaganagar@utsa.edu

relates wind speed to the power output of a single wind turbine. One determines AEP_{gross} using the frequency of wind speeds at a specific site combined with the manufacturer's power curve. This simplistic estimate is used in the conceptual design and as a base for AEP_{net} estimations.

AEP_{net} predictions are important because they help determine whether a wind turbine or wind farm will be financially viable (Tegen et al., 2012). The accuracy of these predictions can be the difference between financial success and failure. A recent survey by Clifton et al. (2016) showed that, on average, preconstruction estimates for AEP were overestimating actual energy production by 6%. The overestimation can have a substantial impact on operators of wind farms if the wind energy infrastructure is oversized. This study also showed that the most prominent variation between different preconstruction estimates was the estimation of wake losses. There is a great need to improve wake loss estimations for AEP_{net} predictions.

The wakes generated behind wind turbines have been of particular interest because they directly affect the power losses in large wind farms. Numerical studies (Abkar and Porté-Agel, 2015; Calaf et al., 2010; Lu and Porté-Agel, 2011; Meyers and Meneveau, 2010; Porté-Agel et al., 2011; Wu and Porté-Agel, 2012), wind tunnel experiments (Chamorro and Porté-Agel, 2009, 2010; España et al., 2011; Hu et al., 2012; Yang et al., 2011), and field studies (Clifton et al., 2013; St. Martin et al., 2016; Vanderwende and Lundquist, 2012; Wharton and Lundquist, 2012a, 2012b) have all shown that atmospheric stability plays a significant role in the dynamics of wakes behind wind turbines (Abkar and Porté-Agel, 2015; Bangga et al., 2018; Churchfield et al., 2012a; Ghaisas et al., 2017; Iungo and Porté-Agel, 2014; Keck et al., 2014; Peña and Rathmann, 2014; Schepers et al., 2001; Xie and Archer, 2017). Current methods for estimating AEP do not wholly capture atmospheric effects of wakes and wake losses (Sohoni et al., 2016) and therefore a significant effort has been performed to better understand stability effects on wind turbine wakes and power production. Wu and Porté-Agel (2012) used large eddy simulation (LES) to study the wakes behind a single wind turbine and showed that increased turbulence from wind shear increased the wake entrainment and wake recovery. Abkar and Porté-Agel (2015) compared wakes under different stabilities and showed that wakes under convective conditions recover faster than those under neutral and stable conditions due to increased turbulence in the inflow. Buoyancy production from increased surface flux generates the turbulence. Similarly, the surface heat flux has been used to simulate wind turbine wakes in the evening transition from unstable conditions. The power ratio, a measure of the simulated power generation to the potential power production given undisturbed inflow, decreased by 15% as the surface heat flux decreases into the evening (Lee and Lundquist, 2017). These studies suggest that surface heat flux has a significant influence on wake effects of the wind turbines.

The study of atmospheric effects on single turbines has led to the study of atmospheric effects on wind turbine arrays including power production. Lu and Porté-Agel (2011, 2015) performed simulations of an infinite wind turbine array for both the stable and convective atmospheric boundary layer (ABL) to show the interactions of wind farms and the atmosphere. Churchfield et al. (2012b) showed that the ratio of power produced from upstream compared to downstream wind turbines is 15%–20% higher when the atmosphere is convective compared to neutral. Ghaisas et al. (2017) looked at power production of a large wind turbine array for stable, neutral, and convective cases. The study showed that increased turbulence in the convective atmosphere not only aided wake recovery but also increased wake expansion. The convective case, therefore, had smaller power losses for downstream turbines in an aligned configuration but more considerable power losses for a staggered arrangement. These concepts aid in understanding the complex findings from different field campaigns because they show that wind direction, wind farm layout, and atmospheric stability are all coupled together in their effects on wind turbine performance (Chamorro and Porté-Agel, 2009, 2010; Porté-Agel et al., 2011). Numerical studies have improved our understanding of the role of atmospheric stability on power production due to the influence of the wakes. There is still a gap between the fundamental knowledge and practical application of the knowledge to improve power predictions in a wind farm. This study is unique as it builds on the theoretical foundation of the atmospheric boundary layer dynamics to evaluate the performance of wind turbines in terms of net energy production with wake losses.

This study investigates the variations in surface heat flux for a convective ABL and their effects on EP_{net} . Nielson and Bhaganagar (2017) used field data from the National Renewable Energy Laboratory (NREL) field campaign of 2015 to determine boundary and initial conditions for LES (including surface heat flux, boundary height). The study observed large seasonal, diurnal, and day-to-day variations in surface heat flux and showed the impact of the variations on the turbulence generated in ABL. The day-to-day variation of peak surface heat flux showed that turbulent kinetic energy (TKE) at +1 standard deviation (SD) was 98% higher than TKE at –1 SD (with respect to surface heat flux). Similarly, Archer et al. (2016) showed large frequencies of unstable and very unstable conditions in the US northeastern coast. The significant variations in atmospheric conditions bring some questions. Is further fidelity of stability required than these three states? And, how can large data sets be used as probabilistic inputs for energy forecasting using LES? These questions represent a gap in the current field of research.

The objectives of this study are as follows:

Table 1. LES precursor simulations performed using PDFs (of surface heat flux) from the NREL July 2015 12 p.m. data.

Precursor simulation	PDF	Surface heat flux (kms^{-1})	Inversion height (m)	Geostrophic wind (ms^{-1})	Obukhov length (m)
1	July mean	0.231	756	9.1	-78
2	July -1 SD	0.116	659	9.1	-89
3	July +1 SD	0.346	820	9.1	-65
4	July mean	0.231	756	6.9	-58

LES: large eddy simulation; PDF: probability density function; NREL: National Renewable Energy Laboratory; SD: standard deviation.

1. To conduct LES to simulate single, double, and triple wind turbine arrays using the mean, -1, and +1 SDs of surface heat flux measured at 12 p.m. in July 2015 from the NREL field site.
2. To validate the wake recovery rates of the single turbine array with LIDAR measurements from Iungo and Porté-Agel (2014).
3. To compare the wake recovery rates, power deficits, and EP_{net} for different surface heat fluxes of the convective ABL.
4. To understand the effect of day-to-day variability of surface heat flux within the context of EP and estimate the net energy production for single, double, and triple wind turbine arrays.

The data used in this study are obtained from the existing NREL National Wind Technology Center (NWTC) field experiment database site (NWTC Information Portal, n.d.). The instrumentation includes sonic anemometers, cup anemometers and vanes, temperature measurements (absolute, differential, and dew point), precipitation measurements, and barometric pressure measurements at different heights and is fully described by Clifton et al. (2013). The NREL data set uses Applied Technologies, Inc. (ATI) (Virginia 22485, USA) “K”-type anemometers to measure the vertical wind speeds, u , v ; the vertical wind speed w ; and the temperature T_s components at 15, 30, 50, 76, 100, and 131 m. The derived variables include the mean wind speeds, wind direction, atmospheric stability, surface fluxes, and boundary layer heights during the convective ABL. The NREL data are captured at a high frequency that allows the use of turbulent quantities in atmospheric calculations and were collected for January, May, July, and October 2016.

The LES has been performed using the Simulator for Wind Farm Applications (SOWFA) solver developed by the NREL. The LES uses ideal assumptions with a homogeneous pressure gradient, flat terrain, and steady conditions (see Churchfield et al., 2010). The field data were used to obtain the surface heat flux, inversion height, and geostrophic wind which are the boundary and initial conditions for the LES solver.

Methodology

The numerical simulations performed consist of two parts, both of which use SOWFA. First, a precursor ABL solver is used to obtain quasi-steady ABL solution for given initial and boundary conditions. The boundary/initial conditions of surface heat flux, geostrophic wind, and initial inversion height are derived from the field data. The precursor simulation generates realistic atmospheric boundary layer turbulence. Second, the wind turbine solver is used with precursor ABL simulation as inflow to obtain a fully turbulent wind turbine simulation that was run to steady state and then averaged for 10 min of actual time. The precursor simulations followed the methodology set forth by Churchfield et al. (2010).

Field data used for LES

The field data from NREL site for July 2015 were used (Clifton, 2007; Clifton et al., 2013; NWTC Information Portal, n.d.). A probability density function (PDF) was derived for each hour of the diurnal cycle. A correlation between inversion height and surface heat flux was developed to set the initial inversion layer height. The simulations were performed with mean surface flux, +1 SD, and -1 SD from the measured surface flux values of the July 12 p.m. data (Nielson and Bhaganagar, 2018). Table 1 shows the precursor simulations performed for the study. The different atmospheric states will be referred to as N1SD for negative 1 SD, Mean1 for the mean with a geostrophic wind speed of 9.1 ms^{-1} , P1SD for the positive 1 SD, and Mean2 for the mean simulation with a geostrophic wind speed of 6.9 ms^{-1} .

LES solver, case study, and definition of parameters

The wind turbine simulations were performed after mapping the precursor fields to a refined mesh. The solver uses the Navier–Stokes equations (1) to (3). The wind turbine simulations add the f_i term in the momentum equation (2) that

represents the force of the wind turbine blade on the fluid. The study utilized the actuator line method (ALM) developed by Sørensen and Shen (2002) to represent this force. The blades were discretized into 40 points each described by a Gaussian distribution that is twice the grid cell length (Lee et al., 2012), and the forces were calculated from a lift and drag table for the corresponding airfoils. The subgrid stresses (SGS) are captured in the τ_{ij} term. The SGS flux and SGS temperature flux are parameterized as $\tau_{ij} - (1/3)\tau_{kk}\delta_{ij} = -v_{SGS}\tilde{S}_{ij}$ and $q_j = -(v_{SGS}/Pr_{SGS})(\partial\tilde{\theta}/\partial x_j)$, respectively (Churchfield et al., 2010). v_{SGS} is the SGS eddy viscosity, and Pr_{SGS} is the turbulent Prandtl number. The SGS temperature flux is computed using Moeng's model (Ayotte et al., 1996). The SGS flux is computed using the Smagorinsky model (Smagorinsky, 1963) as $v_{SGS} = C_s\Delta(2S_{ij}S_{ij})^{1/2}$ where $\Delta = (\Delta x\Delta y\Delta z)^{1/3}$ using the mesh cells in the x , y , and z directions and $C_s = 0.13$ (Ghaisas et al., 2017).

$$\frac{\partial\tilde{u}_i}{\partial x_i} = 0 \quad (1)$$

$$\frac{\partial\tilde{u}_i}{\partial t} = -\frac{\partial}{\partial x_j}\tilde{u}_i\tilde{u}_j - \frac{1}{\rho_o}\frac{\partial\tilde{p}}{\partial x_i} - \frac{\partial\tau_{ij}}{\partial x_j} - f_c\varepsilon_{ij3}\tilde{u}_j + g\left(\frac{\tilde{\theta} - \theta_o}{\theta_o}\right) + f_i \quad (2)$$

$$\frac{\partial\tilde{\theta}}{\partial t} = -\frac{\partial}{\partial x_j}\tilde{u}_j\tilde{\theta} - \frac{\partial q_j}{\partial x_j} \quad (3)$$

SOWFA continues to be validated as improvements are made. Churchfield et al. (2010, 2012a) validated the convective and neutral conditions by comparing mean velocity profiles to previous ABL solvers. Similarly, both Bhaganagar and Debnath (2014) and Ghaisas et al. (2017) validated stable conditions of SOWFA by comparing mean velocity profiles to the GABLS (Beare et al., 2006). Churchfield et al. (2012b) validated the wind turbine portion by comparing the power generated and power deficits of the Lillgrund Wind Farm to numerical simulations.

Both simulations use a similarly sized domain $4000\text{ m} \times 4000\text{ m} \times 2000\text{ m}$. The side boundaries remain periodic for the wind turbine such that the recovered wake recycles into the wind turbine (Frandsen et al., 2006). The precursor simulation grid resolution is 10 m. The precursor simulation is mapped to wind turbine simulation which uses two layers of grid refinement to increase the resolution to 2.5 m in the areas near the wind turbine (Churchfield et al., 2012a). The refined mesh is 3 diameters before the wind turbine, 10 diameters behind the wind turbine, 2.5 diameters to either side, and 2.5 diameters above the wind turbine. The wind turbine used in the simulation is the NREL 5-MW Reference Wind Turbine (Jonkman et al., 2009; Lee et al., 2012). The wind turbine has a 126 m diameter and a hub height of 90 m. A torque controller controls the wind turbine speed during the simulation (Kelley and Jonkman, 2005).

There were three wind turbine configurations used for each precursor simulation: a single wind turbine, a two wind turbines in line, and a three wind turbine triangle array. This study estimates instantaneous power by multiplying the shaft torque and shaft rotational speed (Churchfield et al., 2012b; Ghaisas et al., 2017) of the wind turbine. Figure 1 shows the three-separate arrays. The distance between the first row and second row of wind turbines is five rotor diameters. For the three-turbine array, the second row is spread apart by five rotor diameters but not centered on the first turbine (the spacing is 1.5 diameters and 2.5 diameters in the spanwise direction). It should be noted that there was a 10° difference between the hub height wind directions between the three precursor simulations. The yaw and placement of the single and two-turbine arrays were corrected as such. The three wind turbine array yaw and location were constant for all three precursor simulations, and therefore some deflection in the wakes is observed (Fleming et al., 2014).

The analysis calculates the wake deficit, power deficit, and wake TKE of the wind turbines. The wake deficits and TKE are analyzed using both longitudinal planes (x - y planes) at hub height (Abkar and Porté-Agel, 2015; Wu and Porté-Agel, 2012) and traversal planes at select distances behind the wind turbine (y - z planes) (Iungo and Porté-Agel, 2014; Xie and Archer, 2017). The wake deficit is

$$\text{Wake Deficit} = \frac{(U_{hub_{inflow}} - U_{avg_i})}{U_{hub_{inflow}}} \quad (4)$$

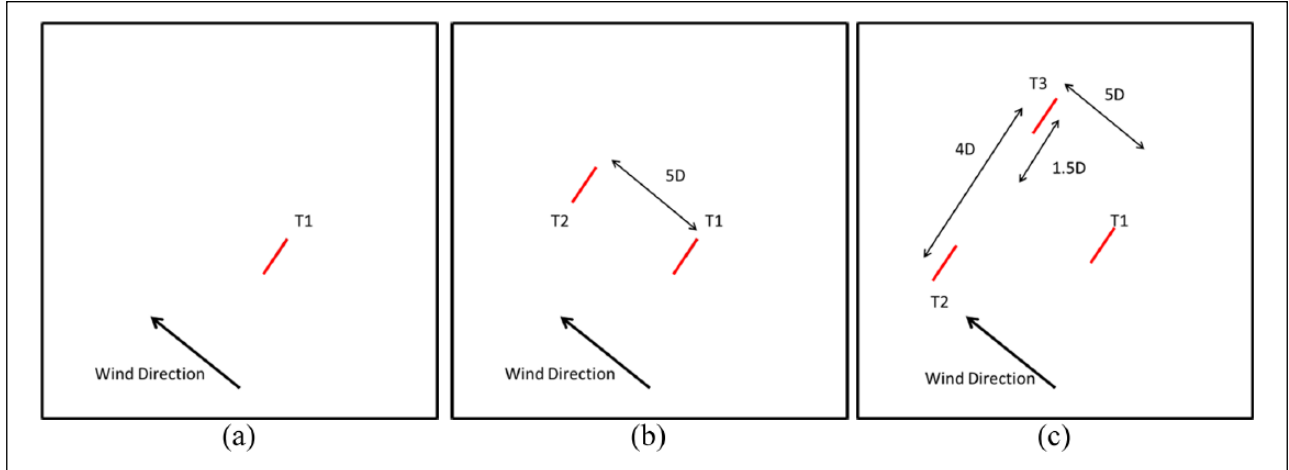


Figure 1. Wind turbine array set up for (a) single turbine array (b) two-turbine array, and (c) three-turbine array.

where $U_{hub_{inflow}}$ is the average velocity at hub height (90 m) in front of the wind turbine, U_{avg_i} is the average velocity at a given distance downstream, and i corresponds to height z_i .

The velocity deficit is used to estimate the wake recovery rate of the wind turbine (Iungo and Porté-Agel, 2014), which is performed by fitting the power law shown in equation (5). The exponent n describes how fast/slow the wake recovers. The wake deficit is

$$\frac{(U_{hub_{inflow}} - U_{min_x})}{U_{hub_{inflow}}} = A \left(\frac{x}{d} \right)^n \tag{5}$$

where U_{min_x} is the minimum velocity in a traversal (y - z) plane distance x behind the wind turbine and d is the diameter of the wind turbine. The curve is fitted using multiple points at different locations downstream to find the constants A and n . The exponent n can be used to define the wake recovery rate of the wake behind the wind turbine. The wake deficits have a negative value for n , which indicates that the wake deficit gets smaller as it progresses downstream. In other words, a negative value of n indicates that the wake is recovering the original state of the atmosphere.

Similarly, power deficits are calculated to compare how much power is being lost by downstream wind turbines

$$Power\ deficit = \frac{(P_{turbine1} - P_{turbine2})}{P_{turbine1}} \tag{6}$$

where $P_{turbine1}$ is the upstream wind turbine and $P_{turbine2}$ is the downstream wind turbine.

In the TKE transport equation, the balance between advection, pressure diffusion, turbulent transport, shear production and buoyancy production of TKE, and dissipation of TKE results in the net TKE. The individual terms are not investigated in this study but rather the TKE is calculated as follows

$$TKE = \frac{1}{2} (\overline{u'_{rms}} + \overline{v'_{rms}} + \overline{w'_{rms}}) \tag{7}$$

where $\overline{u'_{rms}}$ and $\overline{v'_{rms}}$ are the horizontal fluctuations and $\overline{w'_{rms}}$ is the vertical fluctuations. The fluctuations are derived using the root mean square method over the 10-min averaged velocity.

The net energy production is the energy production including losses and is determined as follows:

1. Calculating the gross energy production—The gross energy production is the expected energy output without any losses and is estimated using wind turbine power curves. The gross energy production is calculated using the field data.

2. Predicting the energy losses (e.g. mechanical losses, electrical losses)—For this study, only the wake losses are considered. The wake losses are determined from the LES wind turbine power output.
3. Removing the losses from the gross energy production.

The gross energy production is the expected energy output without any losses and is estimated using wind turbine power curves (Sohoni et al., 2016). The wind turbine power curve is generated by a manufacturer and gives the expected power output of an isolated wind turbine at a given wind speed. The gross energy production is

$$EP_{gross} = \sum f_i P \quad (8)$$

where P_i is the power for a given wind speed and f_i is the frequency of occurrence of the corresponding wind speed. The wind speeds are averaged over each hour and therefore f_i has a unit of hours to get energy from power. To get the annual gross energy production, the total number of frequencies would be 8760 for every hour of the year.

The wake losses are determined using the LES of each case. After the LES is performed, the power for each wind turbine is calculated by multiplying the shaft torque and shaft rotational speed (Churchfield et al., 2012b; Ghaisas et al., 2017) of the wind turbine. The wake of the upstream wind turbine creates lower wind speeds and therefore a reduced power output for downstream wind turbines. The power for the complete wind turbine array (from the LES) is summed as \bar{P}_{net} . P_{gross} is the expected power of the wind turbine array if there were no losses. P_{gross} is calculated using the wind turbine power curve, the hub height wind speed from the LES, and the number of wind turbines in the wind turbine array. Using \bar{P}_{gross} and \bar{P}_{net} , the wake losses are

$$\Delta_{wake} = 1 - \frac{\langle \bar{P}_{net} \rangle}{\langle \bar{P}_{gross} \rangle} \quad (9)$$

The net energy production with wake losses is determined by calculating the gross energy production and removing the wake losses. The gross energy production is determined using equation (8) with the data collected from the NREL meteorological tower. The frequencies f_i are used to match the output of the simulation as described below and therefore do not make a complete AEP. The losses are removed as

$$EP_{net_{wake}} = EP_{gross} (1 - \Delta_{wake}) \quad (10)$$

In general, an AEP is used to estimate the total wind energy developed over a complete year (St. Martin et al., 2016). Therefore, one would estimate the AEP_{gross} with 8760 wind speed events (one for each hour). The study limits the wind speed events to those that match the assumptions of the model. The data used to calculate EP_{gross} are limited to instances that match $\pm 0.3 \text{ ms}^{-1}$ of the average hub height wind speed of the LES simulation and within the surface heat flux bins shown in Figure 2. The mean, +1 SD, and -1 SD surface heat flux results will be used to determine three separate net energy productions with wake losses. These net energy productions for each surface heat flux represent the range based on the variability of the measured surface heat fluxes in the field. An ensemble average will be used to determine a combined net energy production with wake losses using equation (11). Figure 2 shows the weights based on the normal distribution which are 0.3085, 0.383, and 0.3085, respectively

$$AvgEP_{net_{wake}} = w_1 EP_{net_{wake(-1SD)}} + w_2 EP_{net_{wake(-1mean)}} + w_3 EP_{net_{wake(+1SD)}} \quad (11)$$

Similar to the wake losses, one can also quantify the atmospheric inflow effects on the power production of the first wind turbine as in equation (12). A negative number shows that a wind turbine is over-performing compared to the power curve where a positive number indicates that the wind turbine is under-performing. The under-/over-performance has been demonstrated to be associated with the atmospheric inflow conditions (Ghaisas et al., 2017; Vanderwende and Lundquist, 2012; Wharton and Lundquist, 2012b). The Δ_{inflow} is

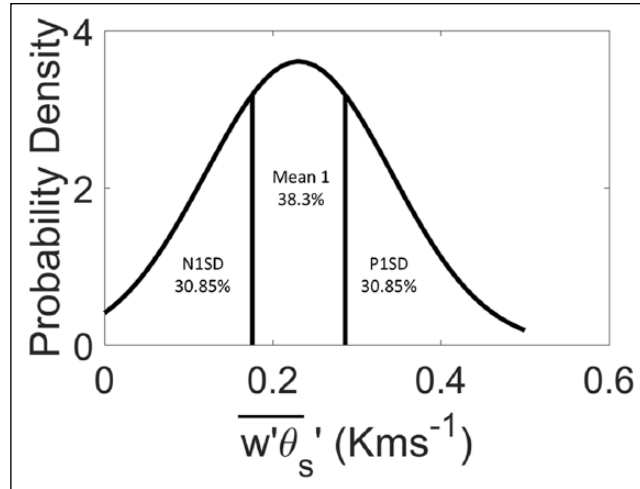


Figure 2. The weights used for N1SD, Mean 1, and P1SD simulations based on the probability density function of surface flux. These weights are used for an ensemble average energy production.

Table 2. LES wind turbine simulation summary.

Simulation	Name	Wind turbine array	Surface heat flux (kms ⁻¹)	Geo. wind (ms ⁻¹)	Obukhov length (m)	EP_{net_wake} (MWh)
1	1Tmean1	1	0.231	9.1	-78	-
2	1Tmean2	1	0.231	6.9	-58	-
3	1TNSD	1	0.116	9.1	-89	-
4	1TPSD	1	0.346	9.1	-65	-
5	2Tmean1	2	0.231	9.1	-78	66
6	2TNSD	2	0.116	9.1	-65	61.6
7	2TPSD	2	0.346	9.1	-89	68.8
8	3Tmean1	3	0.231	9.1	-78	109.6
9	3TNSD	3	0.116	9.1	-65	103.4
10	3TPSD	3	0.346	9.1	-89	111.4

LES: large eddy simulation.

$$\Delta_{inflow} = 1 - \frac{\langle \bar{P}_{net_turbine1} \rangle}{\langle P_{gross_turbine1} \rangle} \tag{12}$$

where $\bar{P}_{net_turbine1}$ is the power of the first wind turbine measured from the LES and $P_{gross_turbine1}$ is the expected power of the first wind turbine. $P_{gross_turbine1}$ is calculated using the wind turbine power curve and the hub height wind speed from the LES.

Results

Table 2 gives a summary of the LES wind turbine simulations performed for the study. The name, number of wind turbines in the array, surface heat flux, geostrophic wind, Obukhov length, and net energy production with wake losses are shown for each LES simulation. The results will refer to the corresponding simulation using the name.

Single wind turbine (isolated WT)

The study analyzes the wind turbine wake recovery by determining the exponent n described in equation (5). Figure 3 shows an example of the power curve fit to the velocity deficit for the 1TMean2 simulation. The graph shows the wake deficit for the minimum velocity for each x distance downstream on a log-log plot along with the fitted curve. The exponent n , or wake recovery rate, was measured to be -0.976 . A typical interval of wake recovery rates for the convective

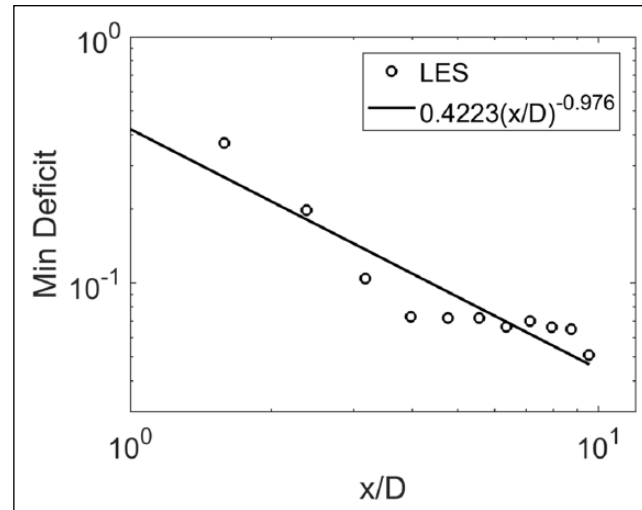


Figure 3. The wake deficit for minimum velocity and downstream distance are shown for the 1TMean2 simulation and the fitted curve. The curve shows the exponent or wake recovery rate to be -0.976 .

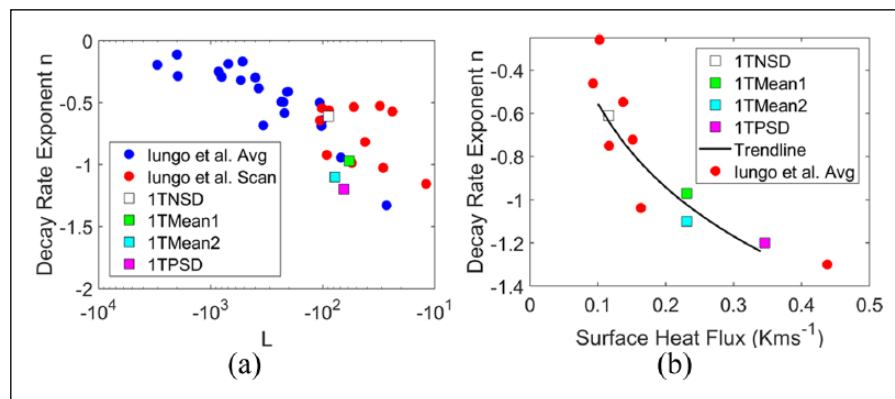


Figure 4. Comparison of wake recovery rates from simulations with lungo and Porté-Agel (a) using Monin–Obukhov length and (b) using surface heat flux.

atmosphere is $[-1.25, -0.25]$ (Iungo and Porté-Agel, 2014). The R^2 value is 0.91 indicating that the power law sufficiently describes the wake behind the wind turbine. The wake recovery rates of all the other simulations were determined in the same manner, and all R^2 values were above 0.88.

The wake recovery rates, exponent n derived from equation (5) as shown in Figure 4, are compared to those measurements made with volumetric LIDAR scanning by Iungo and Porté-Agel (2014) shown in Figure 4. The volumetric LIDAR data include both individual scans and averages of multiple scans as described in the article. Their experiment measured the wakes of an isolated wind turbine in Collonges, Switzerland. They studied the wake deficits for convective and neutral conditions with wind speeds ranging from 4 to 8 ms^{-1} and Monin–Obukhov lengths (L) from -400 to -20 m (where L is $\theta_v u_*^3 / kgw'\theta'_v$). These encompass the ranges from the LES in this study which have hub height velocities of 6.5 to 7.1 ms^{-1} and L of -100 to -50 m. Figure 4(a) shows the wake recovery rate as a function of L . The general trend shows an increase in the recovery rate of the wake of the wind turbine (a more negative exponent) as the atmosphere becomes more convective. The P1SD simulation had a wake recovery rate that was twice as large as the N1SD. The simulations performed agree well with those measured by the volumetric scans, although the LES overestimates the wake recovery rates for the smallest values of Obukhov length. The results agree with wind tunnel experiments (Chamorro and Porté-Agel, 2009) and numerical simulations (Churchfield et al., 2012a; Ghaisas et al., 2017; Wu and Porté-Agel, 2012) that show faster recovery in the convective atmosphere.

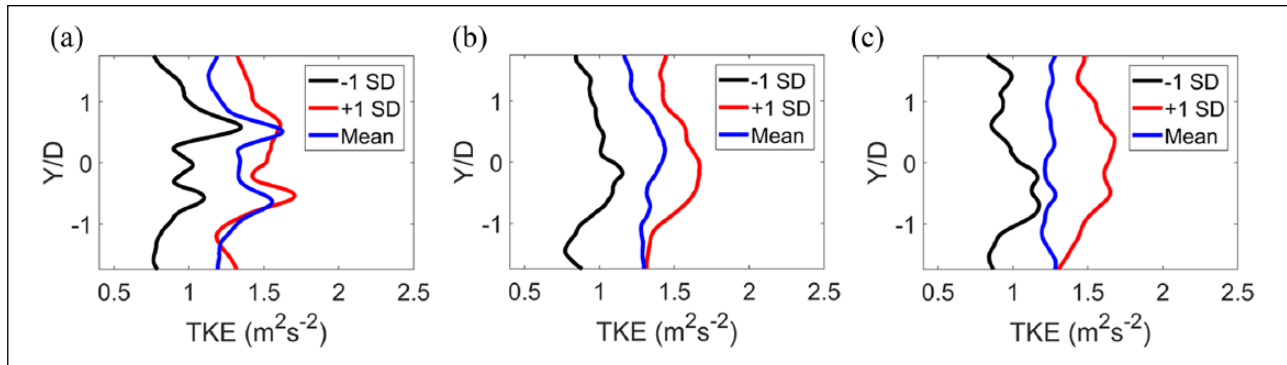


Figure 5. TKE for a single turbine array at (a) 1D, (b) 5D, and (c) 7D.

Figure 4(b) shows the decay rate exponent n versus surface heat flux. The simulations reasonably match those by Iungo and Porté-Agel (2014) (although the values for surface heat flux for the LIDAR data were estimated from the relation of Obukhov length and surface heat flux). The simulations show that for a given geostrophic wind speed, the surface flux significantly affects the wake recovery rate. The wake recovery rate logarithmically decreases with increased surface heat flux. The recovery rate for 1TP1SD is two times as large as that for 1TN1SD. Comparing the 1TMean1 and 1TMean2 simulations, we can also better understand how a change in wind speed affects the wake recovery rate at the same surface heat flux. The wake recovery rate for the Mean1 simulation was 12% larger than that of 1TMean2.

Increased wake recovery occurs due to the increased turbulent mixing in the wakes of the wind turbines. Figure 5 shows the TKE in the wake of the single wind turbine at hub height ($z=90\text{ m}$). Figure 5(a) shows the TKE for the 1TN1SD, 1TMean, and 1TP1SD simulations 1D downstream of the wind turbine. At one rotor diameter downstream, the TKE in the P1SD is approximately 50% larger than the 1TN1SD, but only 10% larger than the Mean1 case. At one rotor diameter downstream of the wind turbine, two peaks are visible at the tips of the blade ($\pm 0.5 Y/D$) (Chamorro and Porté-Agel, 2009). Figure 5(b) shows the TKE for the 1TN1SD, 1TMean, and 1TP1SD simulations 5D downstream of the wind turbine. Further downstream, the TKE in the wakes spreads more evenly, and the 1TP1SD case remains the largest. Figure 5(c) shows the TKE for the 1TN1SD, 1TMean, and 1TP1SD simulations 7D downstream of the wind turbine. At seven rotor diameters downstream, the turbulence of 1TP1SD is still 50% larger than the 1TN1SD case. The added TKE creates the large difference in velocity deficits. The amount of turbulence is largest for 1TP1SD, followed by the 1TMean1, and finally the 1TN1SD. The larger amounts of TKE arise from the background atmospheric inflow (which comes from increased surface heating) which enhances mixing in the wake and help explains the difference in the velocity deficits (Moeng, 1984).

In summary, the isolated wind turbine cases showed a significantly different wake recovery rate for different surface heat fluxes. These values were used to validate the LES with LIDAR measurements from Iungo and Porté-Agel (2014). The faster wake recoveries occurred due to the increased atmospheric turbulence. The turbulence in the wake increased with increased surface heat flux. The effects of wake recovery rates on energy production will be investigated for two and three-turbine arrays.

Two-turbine array

To understand the wake effects, multiple wind turbines are examined. First, the two wind turbine configuration shown in Figure 1 is analyzed. The two wind turbine array provides an understanding of how the increased mixing affects power deficits. Three cases are simulated with boundary conditions as (a) mean surface heat flux 2Tmean1, (b) +1 SD (2TP1SD), and (c) -1 SD (2TN1SD) from mean surface heat flux. Figure 6 shows the power deficit, calculated using equation (6), of the downstream wind turbine for the 2TN1SD, 2TMean1, and 2TP1SD cases. Figure 6(a) shows the power deficit of the downstream wind turbine directly versus surface heat flux. In Figure 6(b), the power deficit of the downstream wind turbine versus the atmospheric stability parameter (z/L) is shown. A larger power deficit means less overall power is produced. The power deficit for the 2TP1SD case is 0.28 compared to 0.46 deficit of 2TN1SD which reasonably falls within that expected from Hansen et al. (2012). The increased wake recovery allows for a more significant amount of the inflow energy for the downstream wind turbine.

The gross energy production is calculated using equation (8) to determine the effect of surface heat flux on energy production. The expected power (determined from the power curve) of the NREL 5 MW wind turbine is between 0.88 and 1.22 MW for hub height wind speeds between 6.5 and 7.1 ms^{-1} ($\pm 0.3\text{ ms}^{-1}$ the hub height wind speed of the simulations)

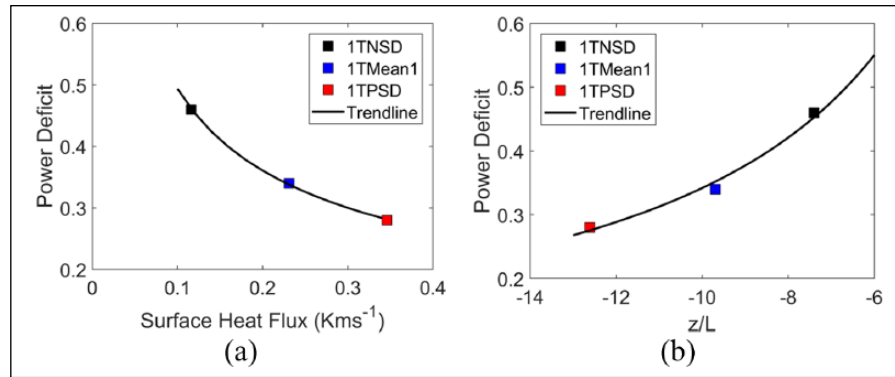


Figure 6. Power deficit data for (a) different surface heat fluxes and (b) different z/L values.

Table 3. Net energy production with wake losses estimation using frequencies field data for a two-turbine array.

Simulation	EP_{gross} (MWh)	Δ_{wake}	Δ_{inflow}	$EP_{net_{wake}}$ (MWh)
2TNISD	80	0.23	-0.074	61.6
2TmeanI	80	0.175	-0.026	66
2TPISD	80	0.14	-0.030	68.8

(Jonkman et al., 2009). The field data had 39 instances that matched assumptions described in the methodology where the hour-averaged hub height wind speed was $\pm 0.3 \text{ ms}^{-1}$ the LES hub height wind speed and the surface heat flux fell in the bin shown in Figure 2. The gross energy production per wind turbine is obtained by summing the expected power from each of the 39 wind speed instances from the field data, and it is 40 MWh. Therefore, the expected energy production for a single wind turbine for the 39 instances is 40 MWh which is used to get the gross energy production of two wind turbines which is 80 MWh.

Table 3 gives the gross energy production EP_{gross} , wake losses Δ_{wake} , inflow effects Δ_{inflow} , and net energy production with wake losses $EP_{net_{wake}}$. The inflow effects are negative for all three simulations which means that a wind turbine is over-performing compared to the power curve as described in equation (11). This finding is supported by the results of Ghaisas et al. (2017) who showed that a wind turbine over-performed in the convective ABL when wind speeds were below 10 ms^{-1} . Vanderwende and Lundquist (2012) showed that the convective power curve for similar wind speeds overproduced by values up to 12% the power curve. The wake losses are determined using the power from the LES using equation (9). The wake losses are then used to determine the net energy production with wake losses using equation (10). There is a 10% difference between the net energy production with wake losses for the two-turbine array between the 2TNISD and 2TPISD. The difference shows that the net energy production forecast significantly changes depending on the atmospheric stability in the convective atmospheric boundary layer. The average net energy production with wake losses is 65.5 MWh using the weights based on the PDF in Figure 2 and equation (11). The ensemble average calculated using the weights is less than that calculated using just the mean because of the more substantial wake loss for the 2TNISD simulation.

To implement the above methodology for a complete net AEP would require significant computational power because a similar set of simulations would be required to be performed for each wind speed. Further computational power would be necessary to include effects of misalignments of the inflow wind direction and different downstream distances.

Figure 7 compares the wake recovery rates of the upstream and downstream wind turbines. Figure 7(a) shows the wake recovery rate versus the surface heat flux for the upstream and downstream wind turbine. Figure 7(b) shows the wake recovery rate versus the atmospheric stability parameter (z/L) for both the upstream and downstream wind turbines. The downstream wind turbine wake recovery rate increases with increased surface heat flux, but at a much smaller magnitude than for the upstream wind turbine due to increased turbulence in the wakes. The wake recovery rates for the downstream wind turbine are within 10% of that measured in the 2TMean1 simulation for the upstream wind turbine. It should also be noted that the recovery rate for the 2TPISD downstream turbine was less than the recovery rate for the upstream wind turbine by 20% which suggests that the variations in surface heat flux would have less of an effect on the power deficits of a third row of wind turbines, which can also be inferred from studies looking at the power deficits of aligned wind turbine arrays. Aligned turbines show an asymptotic nature after the second row of wind turbines (Gaumont et al., 2014).

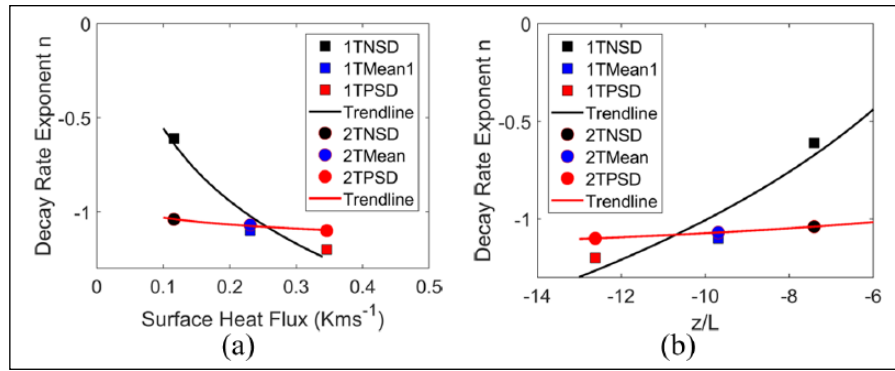


Figure 7. Wake recovery rates for the upstream and downstream wind turbines using (a) surface heat flux and (b) z/L .

Table 4. Net energy production with wake losses estimation using frequencies’ field data for a three-turbine array.

Simulation	EP_{gross} (MWh)	Δ_{Wake}	Δ_{inflow}	$EP_{net_{wake}}$ (MWh)
3TNISD	120	0.138	-0.0018	103.4
3Tmean1	120	0.087	-0.050	109.6
3TPISD	120	0.071	-0.061	111.4

Three-turbine array

The three wind turbine case is analyzed next to understand the effect of staggered arrangement on the energy production. Table 4 gives the gross energy production EP_{gross} , wake losses Δ_{wake} , inflow effects Δ_{inflow} , and net energy production with wake losses $EP_{net_{wake}}$. Similar to the two-turbine array, the results show that the wind turbine is over-performing compared to the power curve due to inflow effects (Ghaisas et al., 2017; Vanderwende and Lundquist, 2012). For all cases, the staggered layout reduced the wake losses from the two-turbine array because the downstream wind turbines are not directly hit with the upstream wake (Ghaisas et al., 2017). Although the wake losses are reduced, they still have a significant effect on net energy production with wake losses. There is an 8% difference in net energy production with wake losses between the 3TP1SD and 3TN1SD cases. The staggered array reduced the wake effects on the energy production estimation. The average net energy production with wake losses is 108.2 MWh when calculated from the PDF weights as shown in Figure 2 and equation (11). Again, the weighted net energy production is smaller than that predicted by just using the mean.

Discussion and conclusion

A novel study has been conducted for the first time to use field-based LES study to evaluate the net energy production of two and three-turbine arrays accounting for the wake effects between the wind turbines. The objectives of this work are to use LES to simulate wind turbines to validate and compare the wake recovery rates, contrast power deficits, and determine the estimated $EP_{net_{wake}}$ for different surface heat fluxes of the convective ABL (measured from the field) as well as an ensemble average.

The $EP_{net_{wake}}$ is determined as follows:

1. Calculating the gross energy production using equation (8)—The gross energy production is the expected energy output without any losses and is estimated using wind turbine power curves. The gross energy production is calculated using the field data.
2. Predicting the energy losses—For this study, only the wake losses are considered and are determined from the LES using equation (9).
3. Removing the losses from the gross energy production using equation (10).

The gross energy production can be estimated for any number of wind turbines by merely multiplying the number of wind turbines. Therefore, the methodology described in the article scales to a large wind farm where the wind farm would be required to be simulated using LES. The losses from the LES wind farm simulation could then be removed from the gross energy production.

LES of a single, double, and triple wind turbine array were performed for full-scale horizontal axis wind turbines. These were simulated under three different instances of surface heat flux in the convective atmospheric boundary layer. The boundary conditions for the LES were obtained from the field data. The surface heat fluxes for the NREL July 12 p.m. were used to get a mean (over 30 diurnal cycles), +1, and -1 SD values for surface heat flux. The field data correlation between surface heat flux and boundary height was used to select the initial inversion height for each surface heat flux. The simulations were determined based on the PDFs from measured data. LES cases for the mean, +1 SD, and -1 SD from the measurements of surface heat flux were performed. Significant differences in wake recovery, wake turbulence, power deficits, and net energy production with wake losses between the three states were observed. The added surface flux increases the turbulence in the atmospheric inflow. This leads to faster wake recovery and enhanced wake turbulence. The larger surface heat flux increases the wake recovery by a factor of two. The increased wake recovery reduces the power deficit by over 20% for the two-turbine array. The study shows the importance of including further fidelity past a single convective stability simulation.

Furthermore, significant differences in net energy production with wake losses are evident. There is a 10% difference in EP_{net_wake} for the two-turbine array between the -1 and +1 SDs from the mean surface flux. The difference in EP_{net_wake} is 8% for the triple-turbine array. Thus, EP_{net_wake} depends on the number of wind turbines, the arrangement of the wind turbine (staggered or not), and the atmospheric stability in convective ABL. The mean, -1 SD, and +1 SD cases represent the range of variations from day to day (in atmospheric stability) that were measured in the field. The large differences in EP_{net_wake} shed light in the uncertainty of EP_{net_wake} based on variations in atmospheric stability that occurs naturally (Nielson and Bhaganagar, 2018). An incorrect assumption about the surface heat flux, from a wide range of measured values, could lead to significant differences in the estimation of energy production for a wind farm. Therefore, it is important to understand the uncertainty by performing multiple LES based on variations measured in the field. The separate simulations can then be combined to generate an ensemble average based on the frequency of occurrence to get a more accurate prediction.

The LES cases were used to generate a weighted average net energy production with wake losses as shown in Figure 2 and equation (11). The weights are applied to the net energy production with wake losses for each surface heat flux (mean, -1 SD, and +1 SD) and then summed. By including the variation of the surface heat flux with the weighted average, the net energy production with wake losses is smaller than using only the mean because of the asymptotic nature of the power deficits due to wake losses, which is one possibility for overestimation from preconstruction estimates (Clifton et al., 2016). The findings show the importance of correctly implementing the surface heat flux variability for wind turbines in convective ABL. This work continues to show the complex effects the atmosphere has on wind turbines. The surface heat flux plays a significant role in the wake recovery rate, power deficit, and AEP_{net} of the wind turbines.

Others have looked at improving AEP forecasting using Monte-Carlo simulations (Gallagher and Elmore, 2009; Hrafnkelsson et al., 2016). This method improved the forecast of wind turbines over normal Weibull distributions because it accounted for seasonal variations and autocorrelations of wind speeds. However, their approach did not contain atmospheric effects. The Monte-Carlo approach of atmospheric stability becomes more practical as LES becomes readily available. The Monte-Carlo simulations could include the wake losses estimated from multiple LES simulations and further improve AEP estimation in the future.

The work is offered as a contribution to improved prediction in net energy production of multiple wind turbines using field-based highly accurate numerical simulation (LES). The work presents a methodology to incorporate frequencies of surface heat flux (representing different stabilities) into AEP estimation. Further fidelity of the convective boundary layer is required to improve AEP forecasting. This study uses a high-fidelity numerical solver that accounts for realistic ABL simulation with surface heat flux measurements from the field to estimate the energy production of wind turbine arrays. The work provides an important direction of using LES for accurate calculation of AEP.

Acknowledgements

The authors would like to acknowledge the Texas Advanced Computing Center for the computer time to perform the simulations. The authors would like to acknowledge the National Renewable Energy Lab for collecting and giving the data from the field site as well as developing the SOWFA code.


Declaration of conflicting interests

The author(s) declared no potential conflicts of interest with respect to the research, authorship, and/or publication of this article.

Funding

The author(s) received no financial support for the research, authorship, and/or publication of this article.

ORCID iD

Jordan Nielson  <https://orcid.org/0000-0002-3411-9558>

References

- Abkar M and Porté-Agel F (2015) Influence of atmospheric stability on wind-turbine wakes: A large-eddy simulation study. *Physics of Fluids* 27: 035104.
- Archer CL, Colle BA, Veron DL, et al. (2016) On the predominance of unstable atmospheric conditions in the marine boundary layer offshore of the U.S. northeastern coast. *Journal of Geophysical Research: Atmospheres* 121: 8869–8885.
- Ayotte KW, Sullivan PP, André A, et al. (1996) An evaluation of neutral and convective planetary boundary-layer parameterizations relative to large eddy simulations. *Boundary-Layer Meteorology* 79: 131–175.
- Bangga G, Guma G, Lutz T, et al. (2018) Numerical simulations of a large offshore wind turbine exposed to turbulent inflow conditions. *Wind Engineering* 42: 88–96.
- Beare RJ, Macvean MK, Holtslag AA, et al. (2006) An intercomparison of large-eddy simulations of the stable boundary layer. *Boundary-Layer Meteorology* 118: 247–272.
- Bhaganagar K and Debnath M (2014) Implications of stably stratified atmospheric boundary layer turbulence on the near-wake structure of wind turbines. *Energies* 7: 5740–5763.
- Calaf M, Meneveau C and Meyers J (2010) Large eddy simulation study of fully developed wind-turbine array boundary layers. *Physics of Fluids* 22: 015110.
- Chamorro LP and Porté-Agel F (2009) A wind-tunnel investigation of wind-turbine wakes: Boundary-layer turbulence effects. *Boundary-Layer Meteorology* 132: 129–149.
- Chamorro LP and Porté-Agel F (2010) Effects of thermal stability and incoming boundary-layer flow characteristics on wind-turbine wakes: A wind-tunnel study. *Boundary-Layer Meteorology* 136: 515–533.
- Churchfield MJ, Lee S, Michalakes J, et al. (2012a) A numerical study of the effects of atmospheric and wake turbulence on wind turbine dynamics. *Journal of Turbulence* 13: N14.
- Churchfield MJ, Lee S, Moriarty PJ, et al. (2012b) A large-eddy simulation of wind-plant aerodynamics. In: *50th AIAA aerospace sciences meeting including the new horizons forum and aerospace exposition*, Nashville, TN, 9–12 January.
- Churchfield MJ, Moriarty PJ, Vijayakumar G, et al. (2010) Wind energy-related atmospheric boundary-layer large-eddy simulation using OpenFOAM. In: *19th symposium on boundary layers and turbulence*, Keystone, CO, 2–6 August.
- Clifton A (2007) *An Unofficial Guide to Data Products from the NWTC 135-m Meteorological Towers*. Golden, CO: National Renewable Energy Laboratory (NREL).
- Clifton A, Schreck S, Scott G, et al. (2013) Turbine inflow characterization at the National Wind Technology Center. *Journal of Solar Energy Engineering* 135: 031017.
- Clifton A, Smith A and Fields M (2016) *Wind Plant Preconstruction Energy Estimates: Current Practice and Opportunities*. Golden, CO: National Renewable Energy Laboratory (NREL).
- España G, Aubrun S, Loyer S, et al. (2011) Spatial study of the wake meandering using modelled wind turbines in a wind tunnel. *Wind Energy* 14: 923–937.
- Fingersh L, Hand M and Laxson A (2006) *Wind Turbine Design Cost and Scaling Model*. Golden, CO: National Renewable Energy Laboratory (NREL).
- Fleming PA, Gebraad PM, Lee S, et al. (2014) Evaluating techniques for redirecting turbine wakes using SOWFA. *Renewable Energy* 70: 211–218.
- Frandsen S, Barthelmie R, Pryor S, et al. (2006) Analytical modelling of wind speed deficit in large offshore wind farms. *Wind Energy* 9: 39–53.
- Gallagher R and Elmore AC (2009) Monte Carlo simulations of wind speed data. *Wind Engineering* 33: 661–673.
- Gaumond M, Réthoré P-E, Ott S, et al. (2014) Evaluation of the wind direction uncertainty and its impact on wake modeling at the Horns Rev offshore wind farm. *Wind Energy* 17: 1169–1178.
- Ghaisas NS, Archer CL, Xie S, et al. (2017) Evaluation of layout and atmospheric stability effects in wind farms using large-eddy simulation. *Wind Energy* 20: 1227–1240.
- Hansen KS, Barthelmie RJ, Jensen LE, et al. (2012) The impact of turbulence intensity and atmospheric stability on power deficits due to wind turbine wakes at Horns Rev wind farm. *Wind Energy* 15: 183–196.
- Hrafnkelsson B, Oddsson GV and Unnthorsson R (2016) A method for estimating annual energy production using Monte Carlo wind speed simulation. *Energies* 9: 286.
- Hu H, Yang Z and Sarkar P (2012) Dynamic wind loads and wake characteristics of a wind turbine model in an atmospheric boundary layer wind. *Experiments in Fluids* 52: 1277–1294.
- Iungo GV and Porté-Agel F (2014) Volumetric LIDAR scanning of wind turbine wakes under convective and neutral atmospheric stability regimes. *Journal of Atmospheric and Oceanic Technology* 31: 2035–2048.
- Jonkman J, Butterfield S, Musial W, et al. (2009) *Definition of a 5-MW reference wind turbine for offshore system development*. Technical report no. NREL/TP-500-38060. Golden, CO: National Renewable Energy Laboratory (NREL).
- Keck R-E, Maré M, Churchfield MJ, et al. (2014) On atmospheric stability in the dynamic wake meandering model. *Wind Energy* 17: 1689–1710.

- Kelley ND and Jonkman BJ (2005) *Overview of the TurbSim Stochastic Inflow Turbulence Simulator*. Golden, CO: National Renewable Energy Laboratory (NREL).
- Lee JC and Lundquist JK (2017) Observing and simulating wind-turbine wakes during the evening transition. *Boundary-Layer Meteorology* 164: 449–474.
- Lee S, Churchfield M, Moriarty P, et al. (2012) Atmospheric and wake turbulence impacts on wind turbine fatigue loadings. In: *50th AIAA aerospace sciences meeting*, Nashville, TN, 9–12 January.
- Lu H and Porté-Agel F (2011) Large-eddy simulation of a very large wind farm in a stable atmospheric boundary layer. *Physics of Fluids* 23: 065101.
- Lu H and Porté-Agel F (2015) On the impact of wind farms on a convective atmospheric boundary layer. *Boundary-Layer Meteorology* 157: 81–96.
- Meyers J and Meneveau C (2010) Large eddy simulations of large wind-turbine arrays in the atmospheric boundary layer. In: *Proceedings of the 48th AIAA aerospace sciences meeting including the new horizons forum and aerospace exposition*, Orlando, FL, 4–7 January, p. 827. Reston, VA: AIAA.
- Moeng C-H (1984) A large-eddy-simulation model for the study of planetary boundary-layer turbulence. *Journal of the Atmospheric Sciences* 41: 2052–2062.
- Nielson J and Bhaganagar K (2017) Convective surface heat flux effects on wind turbine power. In: *International conference on future technologies for wind energy*, Boulder, CO, 24–26 October.
- Nielson J and Bhaganagar K (2018) Capturing day-to-day diurnal variations in stability in the convective atmospheric boundary layer using large eddy simulation. *The Open Atmospheric Science Journal* 12: 107–131.
- NWTC Information Portal (n.d.) NWTC 135-m meteorological towers data repository. Available at: <https://nwtc.nrel.gov/135mData> (accessed 17 October 2018).
- Peña A and Rathmann O (2014) Atmospheric stability-dependent infinite wind-farm models and the wake-decay coefficient. *Wind Energy* 17: 1269–1285.
- Porté-Agel F, Wu Y-T, Lu H, et al. (2011) Large-eddy simulation of atmospheric boundary layer flow through wind turbines and wind farms. *Journal of Wind Engineering and Industrial Aerodynamics* 99: 154–168.
- Schepers G, Barthelmie R, Rados K, et al. (2001) Large off-shore windfarms: Linking wake models with atmospheric boundary layer models. *Wind Engineering* 25: 307–316.
- Smagorinsky J (1963) General circulation experiments with the primitive equations: I. The basic experiment*. *Monthly Weather Review* 91: 99–164.
- Sohoni V, Gupta SC and Nema RK (2016) A critical review on wind turbine power curve modelling techniques and their applications in wind based energy systems. *Journal of Energy* 2016: 8519785.
- Sørensen JN and Shen WZ (2002) Numerical modeling of wind turbine wakes. *Journal of Fluids Engineering* 124: 393–399.
- St. Martin CM, Lundquist JK, Clifton A, et al. (2016) Wind turbine power production and annual energy production depend on atmospheric stability and turbulence. *Wind Energy Science* 1: 221–236.
- Tegen S, Hand M, Maples B, et al. (2012) *2010 Cost of Wind Energy Review*. Golden, CO: National Renewable Energy Laboratory (NREL).
- Vanderwende BJ and Lundquist JK (2012) The modification of wind turbine performance by statistically distinct atmospheric regimes. *Environmental Research Letters* 7: 034035.
- Wharton S and Lundquist JK (2012a) Assessing atmospheric stability and its impacts on rotor-disk wind characteristics at an onshore wind farm. *Wind Energy* 15: 525–546.
- Wharton S and Lundquist JK (2012b) Atmospheric stability affects wind turbine power collection. *Environmental Research Letters* 7: 014005.
- Wu Y-T and Porté-Agel F (2012) Atmospheric turbulence effects on wind-turbine wakes: An LES study. *Energies* 5: 5340–5362.
- Xie S and Archer CL (2017) A numerical study of wind-turbine wakes for three atmospheric stability conditions. *Boundary-Layer Meteorology* 165: 87–112.
- Xydis G, Koroneos C and Loizidou M (2009) Exergy analysis in a wind speed prognostic model as a wind farm siting selection tool: A case study in Southern Greece. *Applied Energy* 86: 2411–2420.
- Yang Z, Sarkar P and Hu H (2011) An experimental investigation on the wake characteristics of a wind turbine in an atmospheric boundary layer wind. In: *Proceedings of the 29th AIAA Applied Aerodynamics Conference*, Honolulu, HI, 27–30 June, p. 3815. Reston, VA: AIAA.